Fine Exudate Detection using Morphological Reconstruction Enhancement

Akara SOPHARAK*, **Bunyarit UYYANONVARA**, **Sarah BARMAN**, **Sakchai VONGKITTIRUX**, and **Nattapol WONGKAMCHANG**, Guest members

ABSTRACT

Exudates are one of the visible signs of diabetic retinopathy and a marker for the presence of coexistent retinal edema. Diabetic retinopathy is a leading cause of vision loss for approximately 50% of patients with diabetic retinopathy. Automatic exudate detection would be useful in order to detect and treat diabetic retinopathy in an early stage. A fine exudate detection method using a morphological technique is presented and its performance is assessed. The sensitivity, specificity and accuracy are used to evaluate the performance. The sensitivity, specificity and accuracy are 88.1%, 99.2% and 99%, respectively. It is found that the proposed method can improve the accuracy of exudates detection significantly over previous methods.

Keywords: Diabetic retinopathy; Exudate; Fine detection; Morphological reconstruction

1. INTRODUCTION

Diabetes is a disease in which the body does not produce or properly use insulin. Diabetes can affect sight by causing cataracts, glaucoma, and most importantly, damage to blood vessels inside the eye, a condition known as diabetic retinopathy. Diabetic retinopathy is a severe and wide spread eye disease which can be regarded as a manifestation of diabetes on the retina. It is a major public health problem and it remains the leading cause of blindness in people of working age (20 to 65 years) [1]-[4]. The appearance of microaneurysms, haemorrhages and exudates represent the degree of disease. From visual inspection, exudates appear to be a yellowish or a white colour with varying sizes, shape and locations. In this paper, we concentrate on exudate detection as a marker for the presence of macular edema. If the exudates extend into the macular area, vision loss can occur [5], [6]. Automatic exudate detection can assist ophthalmologists prevent and treat the disease more efficiently.

Many techniques have been employed to perform exudate detection. B. Ege et al. [1] use a median filter to remove noise and use thresholding to segment bright lesions and dark lesions, perform region growing, and then identify exudate regions with Bayesian, Mahalanobis and nearest neighbor classifiers. C.I. Sanchez et al. [7] combine colour and sharp edge features to detect exudates. D. Usher et al. [8] use a combination of RRGS and adaptive intensity thresholding to detect candidate exudate regions and a neural network is used to classify exudate and non-exudate pixels. X. Zhang and O. Chutatape [9] use local contrast enhancement and Fuzzy C-Mean (FCM) to segment candidate bright lesion areas. SVMs are also used to classify exudates and cotton wool spots. Kavita and Shenbaga [10] propose median filtering and morphological operations for blood vessel detection. They use multilevel thresholding to extract bright regions assumed to be the optic disc or exudates. They detect the optic disc as the converging point of the blood vessels, and then classify the other bright regions as exudates. A. Osarah et al. [11], [12] use fuzzy c-means (FCM) clustering to segment colour retinal images, then a neural network and support vector machines (SVMs) are used to separate exudate and non-exudate areas. Most of the techniques mentioned earlier are applied to images taken where the pupils of the patient are dilated, in which the exudates and other retinal features are clearly visible. All of these techniques are highly sensitive to image contrast. Automatic exudate detection on images acquired without pupil dilation is investigated to provide decision support and to reduce the workload of ophthalmologists.

In order to improve the performance of exudate detection, segmentation enhancement using morphological reconstruction is used. Section 2 describes the detection method. The performances of different classifiers are compared in Section 3. The paper is discussed and concluded in Section 4.

2. METHOD

All the digital retinal images in this study are taken without pupil dilation with a KOWA-7 nonmydriatic retinal camera with a 45 field of view. The images are stored in JPEG image format files (.jpg) with lowest compression rates. The image size is 752 x 500 pixels at 24 bits per pixel. An example of a retinal image containing exudates is shown in Figure 1. Preprocessing steps, including, feature extraction

Manuscript received on June xx, 2010; revised on June xx, 2010.

A. Sopharak is with Faculty of Science and Arts, Burapha University, Chanthaburi Campus, 57 Moo 1, Kamong, Thamai, Chanthaburi 22170, Thailand

E-mail addresses: akara@buu.ac.th

and optic disc detection are described briefly in section 2.1.1. Morphological reconstruction is described in section 2.1.2 and performance measurements are clarified in section 2.3.

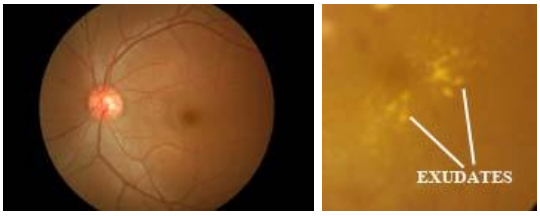

(a) (b)

Fig.1: *(a) a typical normal retinal image (b) cropped retinal image with exudates*

2.1 Exudate Detection

In this paper, we focus on fine-tuned segmentation with a morphological reconstruction technique. The resultant images from previous experiments using FCM clustering [13] are used. The result from FCM clustering is a rough estimation of the exudates; a fine segmentation using morphological reconstruction is applied in order to get an improvement in results.

2.1.1 Preprocessing

Even though the focus of this paper is on the refinement of a previous result using morphological reconstruction, the process of how the result from the previous step was obtained will be discussed briefly in this section. In a pre-processing step, each original RGB image is transformed to HSI colour space. A median filtering operation is then applied on an intensity band to reduce noise. A contrast-limited adaptive histogram equalization (CLAHE) operator [14] is then applied to enhance the local contrast. The optic disc is then removed because it has characteristics similar to exudates. It appears with similar intensity, colour and contrast to other features on the retinal images [15]. The optic disc is detected using the entropy of the preprocessed intensity image [16]. The local pixel intensity entropy measure is high when the region around a pixel is complex and low when it is smooth. After filtering the image with the entropy operator, Otsu's binarization algorithm [17] is applied to separate the complex regions from the smooth regions. The optic disc is then detected by the largest connected component whose shape is approximately circular. Four features are then experimentally selected as input for Fuzzy C-Mean (FCM) clustering. They are the intensity value after pre-processing, the standard deviation of intensity, hue, and the number of edge pixels from an edge image. To calculate the number of edge pixels, we apply a Sobel edge operator then eliminate the strong edges arising from blood vessels and the optic disc using decorrelation stretch [18] on the red band. To determine the suitable number of clusters for FCM clustering, quantitative experiments are performed with a parameter that represents the number of clusters and varies from two to eight.

2.1.2 Mathematical Morphology

The result from the previous step is a rough estimation of the exudates. In order to get a better result, a fine segmentation using morphological reconstruction is applied.

Morphological reconstruction is another major part of morphological image processing. Based on dilation, morphological reconstruction is based on two images, a marker and a mask, rather than one image and a structuring element. The dilation process repeats until it reaches stability; i.e., the image no longer changes.

Morphological reconstruction processes one image, called the marker, based on the characteristics of another image, called the mask. The high-points, or peaks, in the marker image specify where processing begins. The processing continues until the image values stop changing. Conceptually Morphological reconstruction can be thought of as repeated dilations of the marker image until the contour of the marker image fits under the mask image. In this way, the peaks in the marker image "spread out", or dilate. Reconstruction by dilation (the geodesic transformations of an image f (marker) and a second image g (mask)) are shown in Equation 1.

$$R_g(f) = \delta_g^{(i)}(f) \; with \; \delta_g^{(i)}(f) = \delta_g^{(i+1)}(f) \qquad (1)$$

where

$\delta_g^{(n)}(f) = \delta_g^{(n-1)}(f) \; with \; \delta_g^{(1)}(f) = \delta^{(B)}(f) \wedge g$

where $\delta_g^{(n)}$ is a geodesic dilation and B is a flat disc-shaped structuring element with a radius of ten

The cluster which contains exudate areas is used as a marker while the original intensity image is used as a mask. The morphological reconstruction by dilation is then applied on the previous overlaid image. Dilations of the marker image under the mask image are repeated until the contour of the marker image fits under the mask image. The result is displayed in Figure 2 (d).

The final result is obtained by applying a threshold operation at automatically selected grey levels to the difference between the original image and the reconstructed image. The resultant image is shown in Figure 2 (e) and Figure 2 (f) shows the result superimposed on the original image.

2.1.3 Performance Measurement

The performance of our technique is evaluated quantitatively by comparing the resulting extractions with ophthalmologists' hand-drawn ground-truth images pixel by pixel. In order to facilitate the experts to produce a ground-truth image, a first draft of a ground-truth image is created by non-ophthalmologists. The very obvious exudate pixels which are normally bright and yellowish areas were marked pixel by pixel, using a photo manipulation program with one colour. Then, this first draft image is shown to two expert ophthalmologists together with the original image. The ophthalmologists then made some changes by adding some missing exudate pixels and/or removing some misunderstood non-exudate pixels until the ground truth is agreed by both experts.

To evaluate the classifier performance, we use sensitivity, specificity, and accuracy on a per-pixel basis. All measures can be calculated based on four values, namely the true positive (TP) rate (the number of exudate pixels correctly detected), the false positive (FP) rate (the number of non-exudate pixels wrongly detected as exudate pixels), the false negative (FN) rate (the number of exudate pixels not detected), and the true negative (TN) rate (the number of non-exudate pixels correctly identified as non-exudate pixels). These values are defined in Table 1.

Sensitivity is the percentage of the actual exudate pixels that are detected, and specificity is the percentage of non-exudate pixels that are correctly classified as non-exudate pixels. Accuracy is the overall per-pixel success rate of the classifier. From these quantities, the sensitivity, specificity and accuracy are computed using Equation 2 through Equation 4, respectively.

Table 1: *Pixel based evaluation.*

Test Result	Disease Status	
	Present	Absent
Positive	True Positive (TP)	False Positive (FP)
Negative	False Negative (FN)	True Negative (TN)

$$Sensitivity = \frac{TP}{TP + FN} \tag{2}$$

$$Specificity = \frac{TN}{TN + FP} \tag{3}$$

$$Accuracy = \frac{TP + TN}{TP + FP + FN + TN} \tag{4}$$

3. RESULTS

Thirty images are tested on an AMD Athlon 1.25 GHz PC using the MATLAB platform. Each image takes 3 minutes for morphological reconstruction. The result from the coarse segmentation is used as input to the fine segmentation using morphological reconstruction. The sensitivity, specificity and accuracy of validation results are shown in Table 2. A comparison of average result from simple FCM clustering and morphological reconstruction is shown in Table 3.

After fine segmentation, most of the classified exudate regions are true exudates pixels, which give a smaller true positive value; however, it also reduces the false positive value because misclassification of non-exudate pixels is also lower. Figure 3 displays the comparison of exudate detection from FCM clustering and the result of segmentation enhancement using morphological reconstruction and a ground-truth image. Examples of the exudate detection results are shown in Figure 4.

Using morphological reconstruction, gives higher accuracy with a lower false positive values. Compared with FCM clustering, the results indicate that morphological technique performs better in accuracy.

Table 3: *Thetesting results of verifying retinal images.*

Method	Se (%)	Sp (%)	Accuracy (%)
FCM clustering	97.2	85.4	85.6
Morphological reconstruction	88.1	99.2	99.0

4. CONCLUSIONS AND DISCUSSION

In this section, we have investigated and proposed methods to extract exudates from images taken from diabetic patients with non-dilated pupils. The work is based on the morphological reconstruction technique and compared with the result from simple Fuzzy C-Mean clustering.

The performance of the algorithm is measured against ophthalmologists' hand-drawn ground-truths. Three main measurement values, namely, sensitivity, specificity and accuracy are used as the performance measurement of exudates

The result shows that specificity and accuracy values increase when segmentation enhancement using the morphological reconstruction technique is used. There are some incorrect exudate detections which are caused by artifacts that are similar to exudates, artifacts from noise in the image acquisition process, the exudates that are proximate to blood vessels or exudates that appear very faint. These missing faint exudates may have not affected the sensitivity much since even human experts are not sure about some ambiguous regions in the image. However, the performance of the algorithm can be improved if these set of low-contrast exudates can be detected.

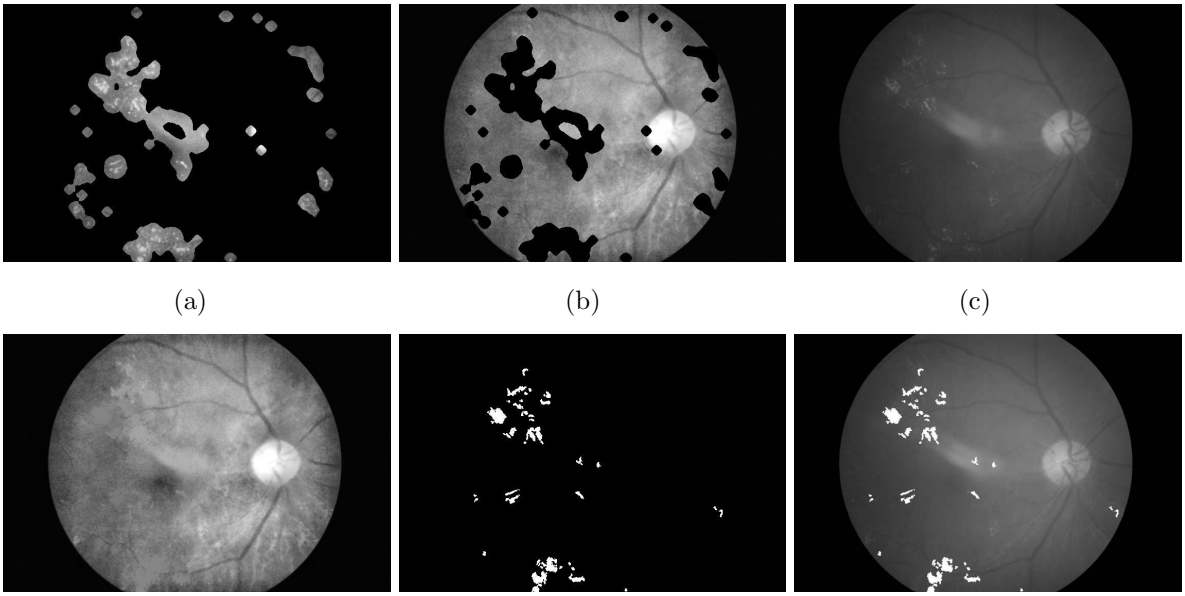

(a) (b) (c)

(d) (e) (f)

Fig.2: *Exudate detection (a) Candidate areas after preprocessing with FCM clustering. (b) Marker image. (c) Mask image. (d) Reconstructed image. (e) Difference image. (f) Result superimposed on the original image.*

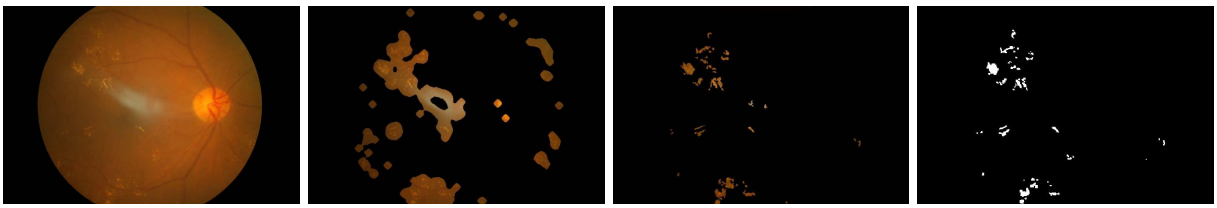

(a) (b) (c) (d)

Fig.3: *Comparison of exudate detection. (a) Original image. (b) Result from preprocessing without morphological reconstruction enhancement (c) Result with morphological reconstruction enhancement. (d) Ground truth image.*

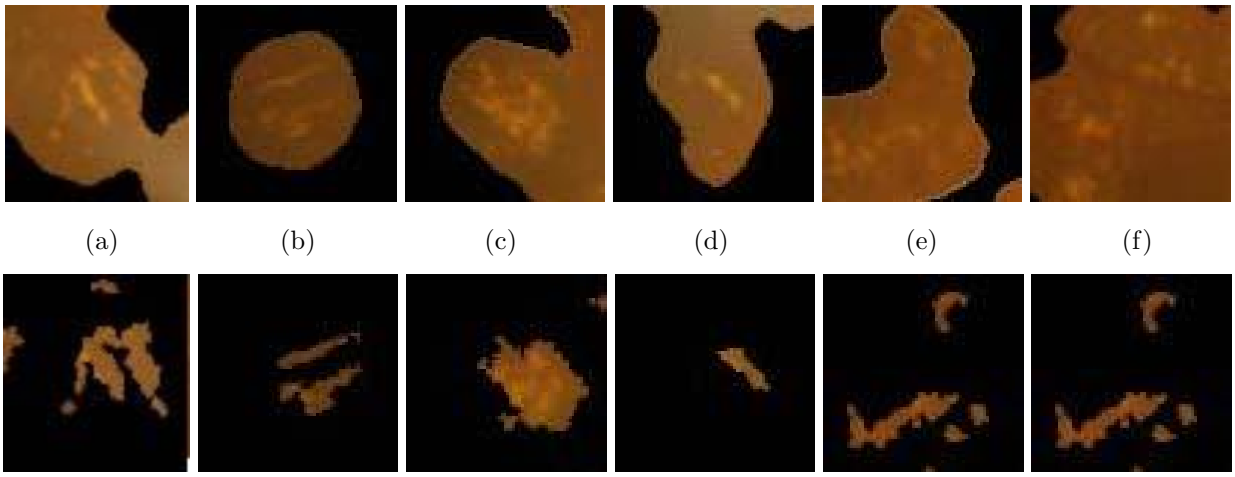

(a) (b) (c) (d) (e) (f)

(g) (h) (i) (j) (k) (l)

Fig.4: *Close-ups of results of exudate detection. (a-f) Result from preprocessing step. (g-l) Result from morphological reconstruction enhancement of figure 4(a-f), respectively.*

Table 2: *The testing results of verifying retinal images from morphological reconsruction.*

24-bit images	TP	FP	FN	TN	Sensitivity (%)	Specificity (%)	Accuracy (%)
Image1	32	1377	5	374586	86.49	99.63	99.63
Image2	903	5301	105	369691	89.58	98.59	98.56
Image3	324	3375	124	372177	72.32	99.1	99.07
Image4	5267	3643	1242	365848	80.92	99.01	98.7
Image5	720	3948	1	371331	99.86	98.95	98.95
Image6	993	1865	57	373085	94.57	99.5	99.49
Image7	177	3452	29	372342	85.92	99.08	99.07
Image8	117	1989	73	373821	61.58	99.47	99.45
Image9	2522	4700	287	368491	89.78	98.74	98.67
Image10	11940	5434	1667	356959	87.75	98.5	98.11
Image11	3026	2462	350	370162	89.63	99.34	99.25
Image12	2684	3343	182	369791	93.65	99.1	99.06
Image13	4898	1677	741	368684	86.86	99.55	99.36
Image14	1019	350	61	374570	94.35	99.91	99.89
Image15	2830	2072	400	370698	87.62	99.44	99.34
Image16	367	1114	15	374504	96.07	99.7	99.7
Image17	23450	7356	1939	343255	92.36	97.9	97.53
Image18	25924	3549	7399	339128	77.8	98.96	97.09
Image19	7057	9486	354	359103	95.22	97.43	97.38
Image20	14718	4397	1037	355848	93.42	98.78	98.55
Image21	2460	5084	385	368071	86.47	98.64	98.55
Image22	3324	3748	266	368662	92.59	98.99	98.93
Image23	2193	1559	93	372155	95.93	99.58	99.56
Image24	8895	1531	1154	364420	88.52	99.58	99.29
Image25	2342	1077	506	372075	82.23	99.71	99.58
Image26	378	2184	75	373363	83.44	99.42	99.4
Image27	747	1788	68	373397	91.66	99.52	99.51
Image28	1239	592	123	374046	90.97	99.84	99.81
Image29	2521	755	385	372339	86.75	99.8	99.7
Image30	249	759	32	374960	88.61	99.8	99.79
Average	**4443.87**	**2998.9**	**638.5**	**367918.73**	**88.1**	**99.19**	**99.03**

5. ACKNOWLEDGMENTS

We thank Thammasat University Hospital for the images and ground truth data used in these experiments. This research is funded by the Thailand National Electronics and Computer Technology Center (NECTEC).

References

[1] B. Ege, O. Hejlesen, O. Larsen, K. Moller, B. Jennings, D. Kerr, and D. Cavan, *Screening for diabetic retinopathy using computer based image analysis and statistical classification,* Comput. Meth. Programs Biomed., vol.62, pp.165-175, 2000.

[2] C. Sinthanayothin, J.F. Boyce, T.H. Williamson, H.L. Cook, E. Mensah, S. Lal, and D. Usher, *Automated detection of diabetic retinopathy on digital fundus image,*. J. Diabet. Med., vol.19, pp.105-112, 2002.

[3] G.G. Gardner, D. Keating, T.H. Williamson, and A.T. Elliott, *Automatic detection of diabetic retinopathy using an artificial neural network: a screening tool.,* British Journal of Ophthalmology, vol.80, pp.940-944, 1996.

[4] Z. Liu, O. Chutatape, and S.M. Krishna, *Automatic image analysis of fundus photograph,* IEEE Conf. on Engineering in Medicine and Biology, vol.2, pp.524-525, 1997.

[5] E.T.D.R.S.R. Group, *Grading diabetic retinopathy from stereoscopic color fundus photographs: an extension of the modified airlie house classi_cation, etdrs report number 10,* Ophthalmology, vol.98, pp.786-806, 1991.

[6] M.D. Davis, S.B. Bressler, L.P. Aiello, N.M. Bressler, D.J. Browning, C.J. Flaxel, D.S. Fong, W.J. Foster, A.R. Glassman, M.E.R. Hartnett, C. Kollman, H.K. Li, H. Qin, and I.U. Scott, *Comparison of time-domain oct and fundus photographic assessments of retinal thickening in eyes with diabetic macular edema.,* Invest Ophthalmol Vis Sci, vol.49, pp.1745-1752, 2008.

[7] C.I. Sanchez, R. Hornero, M.I. Lopez, and J. Poza, *Retinal image analysis to detect and quantify lesions associated with diabetic retinopathy,* IEEE Conf. on Engineering in Medicine and Biology Society, vol.1, pp.1624-1627, 2004.

[8] D. Usher, M. Dumskyj, M. Himaga, T.H. Williamson, S. Nussey, and J. Boyce, *Automated detection of diabetic retinopathy in digital retinal images: A tool for diabetic retinopathy screening,* J. Diabet. Med., vol.21, pp.84-90, 2004.

[9] Z. Xiaohui and O. Chutatape, *Detection and classification of bright lesions in colour fundus images,* IEEE Conf. on Image Processing, vol.1,

pp.139-142, 2004.

[10] Kavitha, D., and Shenbaga Devi, S., 2005, *Automatic detection of optic disc and exudates in retinal images, in: Intelligent Sensing and Information Processing, 2005. Proceedings of 2005 International Conference on,* p. 501-506.Computerized Medical Imaging and Graphics, vol.32, pp.720-727, 2008.

[11] A. Osareh, M. Mirmehdi, B. Thomas, and R. Markham,*Automatic recognition of exudative maculopathy using fuzzy c-means clustering and neural networks,* Medical Image Understanding and Analysis Conference, ed. E. Claridge and J. Bamber, UK, pp.49-52, BMVC Press, 2001.

[12] A. Osareh, M. Mirmehdi, B.T. Thomas, and R. Markham, *Comparative exudate classi_cation using support vector machines and neural networks,* MICCAI '02: Proceedings of the 5th International Conference on Medical Image Computing and Computer-Assisted Intervention-Part II, London, UK, pp.413-420, Springer-Verlag, 2002.

[13] A. Sopharak and B. Uyyanonvara, *Automatic exudates detection from diabetic retinopathy retinal image using fuzzy c-means and morphological methods,* Conf. on Advances in Computer Science and Technology, pp.359-364, 2007.

[14] A. Osareh, M. Mirmehdi, B. Thomas, and R. Markham, *Automated identification of diabetic retinal exudates in digital colour images,* Br. J. of Ophthalmology, vol.87, pp.1220-1223, 2003.

[15] C. Sinthanayothin, J.F. Boyce, H.L. Cook, and T.H. Williamson, *Automated localization of the optic disc, fovea, and retinal blood vessels from digital colour fundus images,* Br. J. Ophthalmal, vol.83, pp.231-238, 1999.

[16] A. Sopharak and B. Uyyanonvara, *Automatic exudates detection from non-dilated diabetic retinopathy retinal image using fuzzy c-means clustering,* Proceedings of the Third WACBE World Congress on Bioengineering, 2007.

[17] N. Otsu, *A threshold selection method from gray-level histogram,* IEEE Transactions on Systems, Man, and Cybernetics, vol.9, pp.62-66, 1979.

[18] S.L. Phung, A. Bouzerdoum, and D. Chai, *Skin segmentation using color pixel classication: Analysis and comparison,* IEEE Transactions on Pattern Analysis and Machine Intelligence, vol.27, pp.148-154, 2005.

Akara Sopharak received her BSc, MSc degrees in computer science and PhD degree in Information Technology from Burapha University, Mahidol University and Sirindhorn International Institute of Technology, Thammasat University Thailand, in 1998, 2002 and 2009 respectively. She is currently an instructor with Faculty of Science and Arts of Burapha University. Her research interests are medical image processing and image analysis.

Bunyarit Uyyanonvara received his PhD in Medical Image Analysis from King's College, London in 2000 and a BSc of Science (1st Class Honours) from Prince of Songkhla University, Thailand. He is now an associate professor at Sirindhorn International Institute of Technology, Thammasat University, Thailand.

Sarah Barman received her PhD in Optical Physics from King's College, London in 1996. She obtained an MSc in Applied Optics from Imperial College London and a BSc in Physics from Essex University. She is now a Principal Lecturer at the Digital Imaging Research Centre in the Faculty of Computing, Information Systems and Mathematics at Kingston University.

Sakchai Vongkittirux is a head of the department of Ophthalmology at Thammasat university hospital, Thailand. He trained and received his medical degrees from Ramathibodi Hospital, Mahidol University and Chulalongkorn University. He is also author of many major Thai text books for ophthalmologist.

Nattapol Wongkamchang is a consultant ophthalmologist of the department of Ophthalmology at Thammasat university hospital, Thailand. He has been working with the research in this field for many years.